Journal of Zhejiang University-SCIENCE A (Applied Physics & Engineering)
ISSN 1673-565X (Print); ISSN 1862-1775 (Online)
www.zju.edu.cn/jzus; www.springerlink.com
E-mail: jzus@zju.edu.cn

Synthesis and characterization of magnetic porous Fe_3O_4/poly(methylmethacrylate-*co*-divinylbenzene) microspheres and their use in removal of Rhodamine B*

Jie SHAN, Li WANG†‡, Hao-jie YU, Yu-lei TAI, Muhammad AKRAM

(*State Key Laboratory of Chemical Engineering, Department of Chemical and Biological Engineering, Zhejiang University, Hangzhou 310027, China*)

†E-mail: opl_wl@dial.zju.edu.cn

Received Apr. 24, 2015; Revision accepted July 1, 2015; Crosschecked July 20, 2015

Abstract: Porous polymers are very suitable materials for the adsorption of organic pollutants due to their abundant pores and organic frameworks in aqueous solution. However, their recovery from treated pollutant is difficult, and thus, their application is limited. A facile strategy to synthesize reusable magnetic porous microspheres (MPMS) of Fe_3O_4/poly(methylmethacrylate (MMA)-*co*-divinylbenzene (DVB)) is described in this paper. The magnetic microspheres were synthesized by suspension co-polymerization. MMA was used as a monomer, DVB was used as a crosslinker, and the magnetic fluid was added to the organic phase. The morphology of MPMS was observed by scanning electron microscope (SEM) and other properties were tested by superconducting quantum interference device, Fourier transform infrared (FT-IR) spectroscopy, thermogravimetric analysis (TGA), X-ray powder diffraction (XRD), and nitrogen sorption-desorption techniques. The synthesized MPMS possessed a high specific surface area using toluene as a porogen. It was further found that the ratio of DVB to MMA, the ratio of porogen to monomer, and the type of porogen all affected the specific surface area and the morphology of the microspheres. Furthermore, the microspheres were applied to remove Rhodamine B from its aqueous solution. The results showed that the microspheres possessed good adsorption capacity for Rhodamine B. This result was due to the porous structure, polar groups, and superparamagnetic characteristic of the synthesized microspheres.

Key words: Fe_3O_4/poly(methylmethacrylate-*co*-divinylbenzene), Porous structure, Suspension polymerization, Dye removal
doi:10.1631/jzus.A1500096 **Document code:** A **CLC number:** TQ584.2

1 Introduction

Dyes are widely used in modern industries, such as paper industry, textile industry, leather industry, rubber industry, plastic industry, cosmetic industry, and so on (Ahmed *et al.*, 2013; Gao *et al.*, 2013). Dyes in the waste water may cause damage to aquatic or even human health. Thus, the removal of dyes from the effluent attracted great attention of researchers. In the past several decades, large amounts of methods have been used to treat dyes in effluent like the coagulation method (Liang *et al.*, 2014; Zhao *et al.*, 2014), chemical oxidation method (Palma-Goyes *et al.*, 2014), catalytic degradation method (Tang *et al.*, 2014; Debnath *et al.*, 2015; Luo *et al.*, 2015), biodegradation method (Adnan *et al.*, 2014; Almeida and Corso, 2014), and adsorption method (Cheng *et al.*, 2015; Filice *et al.*, 2015; Zolgharnein *et al.*, 2015). Among the above-mentioned methods, adsorption is one of the most widely used ones due to low cost, ease of operation,

‡ Corresponding author
* Project supported by the Science and Technology Program of Zhejiang Province (No. 2013C31146), the State Key Laboratory of Chemical Engineering (No. SKL-ChE-12D02), the Science and Technology Innovation Team of Ningbo (No. 2011B82002), and the Fundamental Research Funds for the Central Universities (No. 2015FZA4025), China
ORCID: Jie SHAN: http://orcid.org/0000-0001-5839-2121; Li WANG: http://orcid.org/0000-0001-9356-9930

high efficiency, and insensitivity to toxic materials. Till now, various adsorbents such as activated carbon (Namasivayam and Kavitha, 2002; Hameed *et al.*, 2007), zeolite (Meshko *et al.*, 2001; Wang *et al.*, 2006), clay materials (Vimonses *et al.*, 2009; Garrido-Ramirez *et al.*, 2010), and natural and synthesized polymeric materials (Crini, 2005; Jarvis and Majewski, 2014; Fu *et al.*, 2015) have been used to remove organic dyes from waste water. Although these adsorbents have shown good results in the adsorption of dyes from their waste water, there are limitations such as complexity and high cost of the synthesis procedures, sometimes low adsorption capacities, and most importantly, lack of reusability. Thus, it is a major challenge to develop new types of efficient and reusable adsorbents.

In recent years, porous magnetic materials, especially the Fe_3O_4-based porous materials, have attracted intense attraction in the research of dye adsorption area due to their good reusable property. A lot of effort has been spent in the design and synthesis of magnetic porous materials composed of Fe_3O_4 and inorganic or polymeric porous materials (Yan and Wang, 2014; Khoobi *et al.*, 2015; Wang *et al.*, 2015; Zolgharnein *et al.*, 2015). The Fe_3O_4-based magnetic porous particles are now a promising candidate in the adsorption of dyes because they combine the good porosity of polymers that can be synthesized according to the design and the reusability because of the magnetism of Fe_3O_4. Mak and Chen (2004) synthesized polyacrylic acid (PAA)-coated Fe_3O_4 particles and found out that this material showed efficient adsorption/desorption ability of methylene blue (MB) from its aqueous solution using PAA as the ionic exchange group. In the abovementioned methods, the adsorption is specific because of the affinity of functional group of polymers with different dyes. Liu *et al.* (2010) synthesized porous magnetic microparticles using sulfonated macroporous polydivinylbenzene as a template following ferrous ion exchange and oxidation procedures. Although the synthesized particles had combined characteristics of porosity and affinity of the cationic dyes, the synthesis procedure is considered to be difficult. Thus, a simply synthesized and widely applicable magnetic polymeric adsorbent of dye is needed.

We report a simple approach for synthesizing porous magnetic Fe_3O_4/poly(methylmethacrylate (MMA)-*co*-divinylbenzene (DVB)) supermagnetic microspheres with the existence of oleic acid-coated Fe_3O_4 via modified suspension polymerization of MMA and DVB in this study. A series of experiments were conducted to investigate the controlling factors of the porous structure of polymer. Furthermore, the synthesized microspheres were applied in the adsorption of Rhodamine B from its aqueous solution.

2 Materials and methods

2.1 Materials

MMA was obtained from Sinopharm Chemical Reagent Co. Ltd., China. It was then pretreated as follows: first, it was washed with 10% aqueous solution of sodium hydroxide, then it was dried by anhydrous magnesium sulfate, and finally, it was distilled under a reduced pressure. DVB (80% grade) was obtained from Sigma-Aldrich Chemie GmbH, Germany and treated by passing through the alkaline alumina column to remove inhibitors. Poly(vinyl alcohol) (PVA) (88% hydrolyzed, Mn~88 000) was obtained from Aldrich Chemical Co. and used without pretreatment. Benzoyl peroxide (BPO) was obtained from Sinopharm Chemical Reagent Co., Ltd., China and refined by recrystalization from water. Rhodamine B was obtained from Aladdin Chemistry Co., Ltd., China and used without further purification. Ferric chloride hexahydrate ($FeCl_3{\cdot}6H_2O$), ferrous chloride tetrahydrate ($FeCl_2{\cdot}4H_2O$), aqueous ammonia (25%), sodium chloride, toluene, cyclohexane, and oleic acid were obtained from Sinopharm Chemical Reagent Co., Ltd., China and used without further purification.

2.2 Preparation of oleic acid-coated Fe_3O_4 magnetic fluid

Oleic acid-coated Fe_3O_4 magnetic fluid was prepared by a conventional co-precipitation method (Chen *et al.*, 2009). A three-necked, round-bottom flask reactor was installed with a mechanical stirrer and a reflux condenser with an argon gas inlet tube; then $FeCl_3{\cdot}6H_2O$ (24 g) and $FeCl_2{\cdot}4H_2O$ (9.8 g) were dissolved in 100 ml of deionized water in the flask under nitrogen gas protection with vigorous stirring at 80 °C for 30 min. Then 50 ml of 25% $NH_3{\cdot}H_2O$ was rapidly added to the previously dissolved

solution. After 30 min, 5 ml of oleic acid was added dropwise to the suspension within 10 min. Then the suspension was heated for 1.5 h at 80 °C. After the reaction finished, the black precipitate was separated by a magnet, and then it was washed with deionized water and ethanol for several times to remove the remaining oleic acid. Finally, the magnetic precipitate was redispersed in octane to form magnetic fluid for the next step.

2.3 Preparation of Fe_3O_4/poly(MMA-*co*-DVB) magnetic porous microspheres

Fe_3O_4/poly(MMA-*co*-DVB) magnetic porous microspheres (MPMS) were synthesized by a modified suspension polymerization (Tang *et al.*, 2007). In a typical experiment, a mixture of 10.6 ml of MMA, 1.40 ml of DVB, 3 ml of toluene, and 2.0 g of as-synthesized magnetic fluid were mixed and used as the oil phase, and 2.5 g of PVA and 3 g of NaCl were dissolved in 100 ml of deionized water and used as the water phase. Then, the two phases were mixed in a 250 ml three-necked, round-bottomed flask reactor installed with a mechanical stirrer and a flux condenser with an argon gas inlet tube. Then the mixture was stirred for 30 min under argon gas protection at the room temperature to form a stable oil/water emulsion solution. Afterward, the temperature was increased to 70 °C, and then 0.3 g of BPO was added to initiate the polymerization. The reaction was carried out at 70 °C for 5 h, and a brown magnetic emulsion was obtained finally. After the reaction finished, the obtained black precipitate, MPMS, was separated by magnetic separation with a magnet and then was washed with deionized water and ethanol several times separately to remove the unreacted impurities.

2.4 Characterization

The chemical composite, which is to say the existence of oleic acid, MMA, and DVB in the as-synthesized MPMS, was examined by a Fourier transform infrared (FT-IR) spectrophotometer (Nicolet 5700) using pressed pellets method. The morphology of the MPMS was observed by scanning electron microscope (SEM) (Hitachi S-4800). The SEM samples were coated with gold before testing. The internal structure was observed by transmission electron microscopy (TEM) (JEOL 1200EX). The TEM samples were obtained by dropping the ethanol solution of the samples on carbon-coated copper grids. The porosity of the samples was quantified by Hg intrusion method (Micromeritics' AutoPore IV 9500). The magnetization curves of the MPMS were measured with a superconducting quantum interference device (SQUID) at the room temperature. The crystallinity of the MPMS was examined by X-ray powder diffraction (XRD) analysis. It was carried out on a D/max-rA diffractometer using Cu-Kα radiation with a scan rate of 4 °/min from 10° to 90°. The amount of the polymer incorporated into the MPMS was examined by thermogravimetric analysis (TGA) (Perkin-Elmer TGA-7). The heating rate was 15 °C/min, and the temperature range was from 35 °C to 600 °C.

2.5 Adsorption and desorption tests toward Rhodamine B

The adsorption property of the synthesized particles to Rhodamine B was examined as is described in the following. First, 0.05 g of the as-synthesized MPMS was washed with 1.0 ml of methanol and deionized water three times to make them wet. Then the wet MPMS was added to 5 ml of aqueous solution of a certain concentration of Rhodamine B in a glass bottle. Afterwards the mixture system was dispersed by ultrasonic treatment for 5 min for sufficient interaction between MPMS and Rhodamine B particles. The MPMS saturated with Rhodamine B solution was then separated with a magnet and the concentration of Rhodamine B solution was determined using UV-visual spectroscopy at a wavelength of 554 nm. The desorption test was done by dispersing the MPMS containing Rhodamine B into the ethanol solution by ultrasonic treatment for 5 min, and the concentration of the Rhodamine B ethanol solution was determined once again with UV-visual spectroscopy at a wavelength of 554 nm.

3 Results and discussion

3.1 Fabrication of Fe_3O_4/poly(MMA-*co*-DVB) magnetic porous microspheres

Magnetic porous poly(MMA-*co*-DVB) microspheres were synthesized by modified suspension polymerization method as mentioned in Section 2

(Tang *et al.*, 2007). The illustration of the synthesis procedure is speculated and shown in Fig. 1. The synthesis conditions of the MPMS are shown in Table 1.

3.2 Properties of the synthesized microspheres

3.2.1 Morphology of the synthesized microspheres

The SEM images of samples 1–9 are shown in Fig. 2. Samples 1–3 are the blank samples without Fe_3O_4 inside. As shown in Fig. 2, with the decrease in the amount of crosslinking agent DVB, the morphology of the particles turned from microspheres to amorphous structures (compare A_1, B_1, and C_1). As illustrated in Fig. 1, two reasons were speculated to be the cause of porosity. First, during the polymerization of DVB and MMA, a crosslinked structure was formed, thus helping in forming a macroscopic porous structure; second, the organic solution such as toluene or cyclohexane reacted as a porogen and caused phase separation during polymerization, finally leading to the formation of porous structure (Macintyre and Sherrington, 2004).

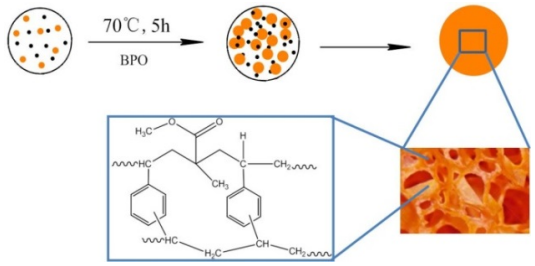

Fig. 1 Schematic drawing of the preparation of porous Fe_3O_4/poly(MMA-*co*-DVB) microsphere and its pore structure

● MMA and DVB; · porogen; ● nuclei of poly(MMA-*co*-DVB)

Comparing A_1 and D_1, we can obtain the conclusion that with the addition of Fe_3O_4 fluent, the surface of the microspheres became more porous. This phenomenon is because the magnetic fluent reacted as the inhibition agent during the formation of the microspheres. Comparing D_3, E_3, and F_3, we find that with the decreasing of the crosslinking agent DVB, the synthesized microspheres turned from porous microspheres to amorphous composites.

To illustrate the effect of the solvent on the synthesized microspheres, we choose the condition containing the smallest amount of the crosslinking agent DVB. The solvent in the system acted as a porogen that creates pores when it is extracted from the system. Normally, the types of porogen are divided into two groups. In the first category, porogens show good thermodynamic compatibility with the incipient polymer network, which can dissolve both monomers and polymers, and in the secondary category, porogens show bad thermodynamic compatibility with the incipient polymer network, which can only dissolve the monomers (Macintyre and Sherrington, 2004). It is believed that a good solvent for the polymer tends to produce expanded networks, resulting in micropores that will collapse when the solvent is removed. The poor solvent for the polymer produces large fixed pores (Rabelo and Coutinho, 1993). In our experiment, we choose toluene as an example of a good solvent and cyclohexane as a poor solvent. Comparing F_1, H_1, and I_1 (the SEM images for

Table 1 Synthesis conditions of porous spheres

Run	Oil phase					Water phase			T (°C)	t (h)	Rotation speed (r/min)
	BPO (g/mmol)	MMA (ml/mol)	DVB (ml/mol)	Porogen (ml)	Magnetic fluent (g)	NaCl (g/mol)	PVA (g/mmol)	H_2O (ml)			
1	0.30/1.24	10.60/0.10	1.40/9.90	3.00[a]	0	3.00/0.050	2.50/0.0284	100	70	5	300
2	0.30/1.24	10.60/0.10	0.26/1.90	3.00[a]	0	3.00/0.050	2.50/0.0284	100	70	5	300
3	0.30/1.24	10.60/0.10	0.13/0.90	3.00[a]	0	3.00/0.050	2.50/0.0284	100	70	5	300
4	0.30/1.24	10.60/0.10	1.40/9.90	3.00[a]	2	3.00/0.050	2.50/0.0284	100	70	5	300
5	0.30/1.24	10.60/0.10	0.26/1.90	3.00[a]	2	3.00/0.050	2.50/0.0284	100	70	5	300
6	0.30/1.24	10.60/0.10	0.13/0.90	3.00[a]	2	3.00/0.050	2.50/0.0284	100	70	5	300
7	0.30/1.24	10.60/0.10	0.13/0.90	3.00[b]	2	3.00/0.050	2.50/0.0284	100	70	5	300
8	0.30/1.24	10.60/0.10	0.13/0.90	6.00[a]	2	3.00/0.050	2.50/0.0284	100	70	5	300
9	0.30/1.24	10.60/0.10	0.13/0.90	9.00[a]	2	3.00/0.050	2.50/0.0284	100	70	5	300

[a] Toluene; [b] cyclohexane

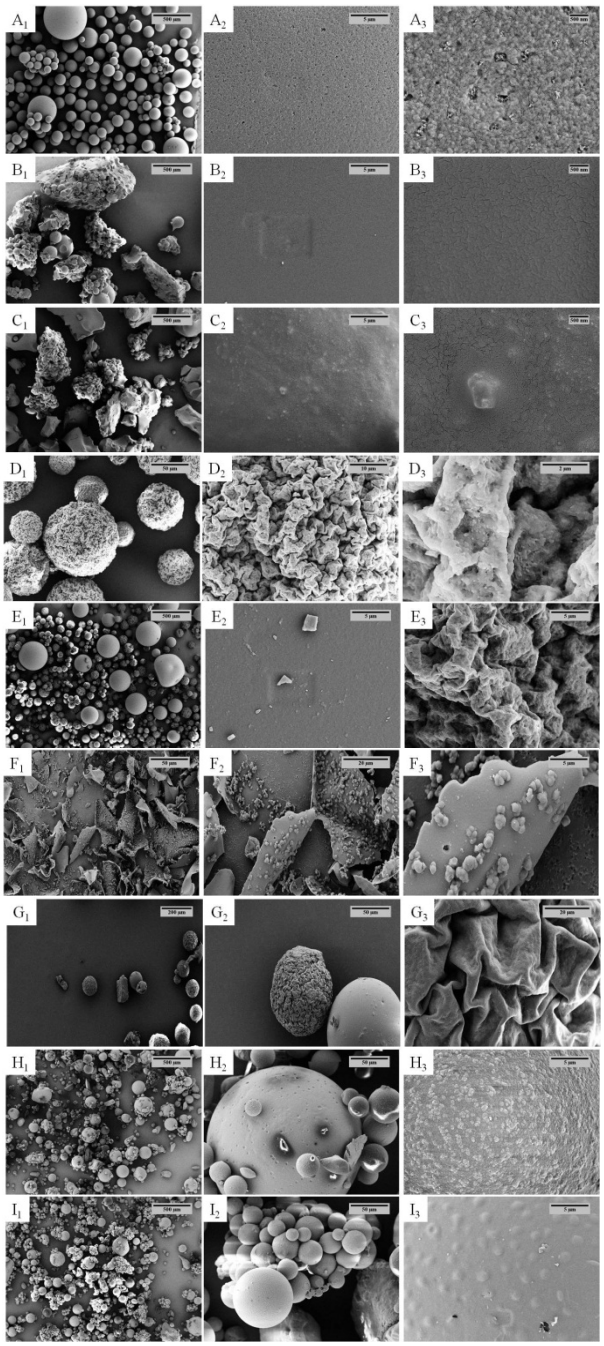

Fig. 2 SEM images of sample 1 (A_1–A_3), sample 2 (B_1–B_3), sample 3 (C_1–C_3), sample 4 (D_1–D_3), sample 5 (E_1–E_3), sample 6 (F_1–F_3), sample 7 (G_1–G_3), sample 8 (H_1–H_3), and sample 9 (I_1–I_3)

samples 6, 8, and 9, respectively) in Fig. 2, it can be found that the synthesized composite turned from amorphous structures to microspheres with little porous surface. This result showed that the solvent played an important role in the formation of poly(MMA-*co*-DVB). With the increase in the amount of the solvent, the tension of the polymer system tends to be more stable to form microspheres.

3.2.2 Chemical composition and crystalline structure of the synthesized microspheres

The chemical composition and crystalline structure of the synthesized microspheres were demonstrated by FT-IR (Fig. 3), EDX result (Fig. 4), and XRD pattern (Fig. 5), respectively. In Fig. 3a, the strong peaks in 600 cm^{-1}–1000 cm^{-1} region are assigned to the C=C groups of DVB and the peak shown at 1770 cm^{-1} is the characteristic adsorption peak of the C=O groups of MMA monomer (Ning, 2000). As can be seen in Fig. 3b, the absorption peak at around 580 cm^{-1} is the characteristic peak for Fe–O which shows the existence of Fe_3O_4 in the microspheres (Mao *et al.*, 2014). Compared with the bare Fe_3O_4 spheres, four new bands at 1457 cm^{-1}, 1523 cm^{-1}, 2852 cm^{-1}, and 2922 cm^{-1} appeared in the FT-IR spectrum of Fe_3O_4/oleic acid spheres. The bands at 2852 cm^{-1} and 2922 cm^{-1} are attributed to the asymmetric $–CH_2$ stretch and the symmetric $–CH_2$ stretch in oleic acid, respectively, and the two bands at 1457 cm^{-1} and 1523 cm^{-1} are attributed to the asymmetric ($–COO^–$) stretch vibration and symmetric ($–COO^–$) stretch vibration, respectively (Li *et al.*, 2010).

In Fig. 4, the EDX images of sample 8 and sample 4 show very clearly the existence of elements Fe, O, and C, which demonstrates the composition of the Fe_3O_4 core and the polymer shell.

Fig. 5 shows the XRD pattern of sample 6. In Fig. 5, all the diffraction peaks can be indexed to face-centered cubic structure of magnetite according to JCPDS card No. 19-0629, which indicates that the coating did not influence the crystal structure of the Fe_3O_4 core.

The five characteristic diffraction peaks of Fe_3O_4 located at 30.2, 35.8, 43.3, 57.2, and 62.6 are assigned to the planes of (220), (311), (400), (511), and (440), respectively (Li *et al.*, 2010).

3.2.3 Coating amount of the polymer shell of the synthesized microspheres

The amount of the polymer shell coated on the Fe_3O_4 core is determined by TGA and its derivative curves (DTG) (Fig. 6).

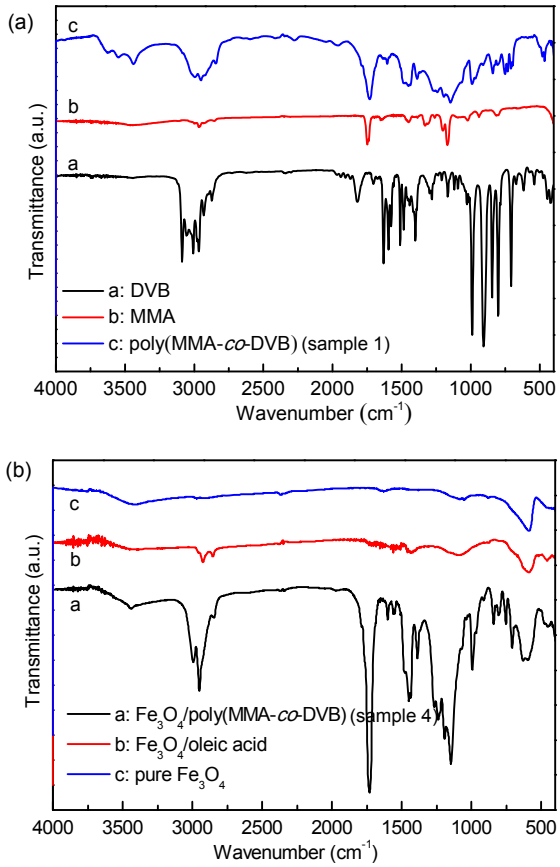

Fig. 3 FT-IR spectra of MMA, DVB, and poly(MMA-*co*-DVB) (sample 1) (a) and pure Fe_3O_4, Fe_3O_4/oleic acid, and Fe_3O_4/poly(MMA-*co*-DVB) (sample 4) (b)

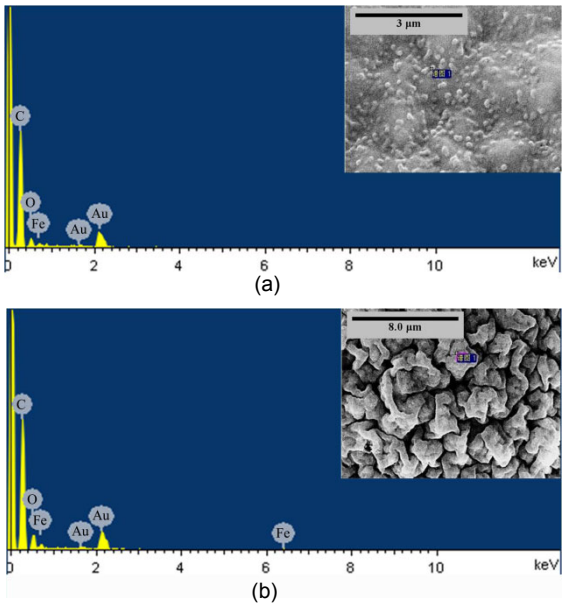

Fig. 4 EDX spectra of sample 8 (a) and sample 4 (b) (insertions are the SEM images)

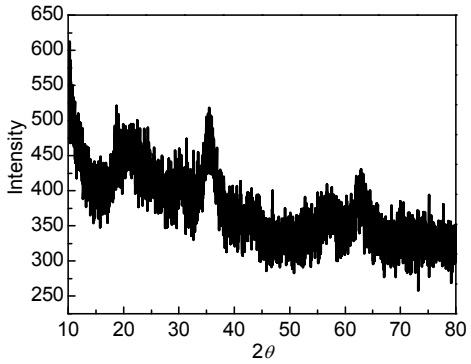

Fig. 5 Powder X-ray diffraction pattern of sample 6

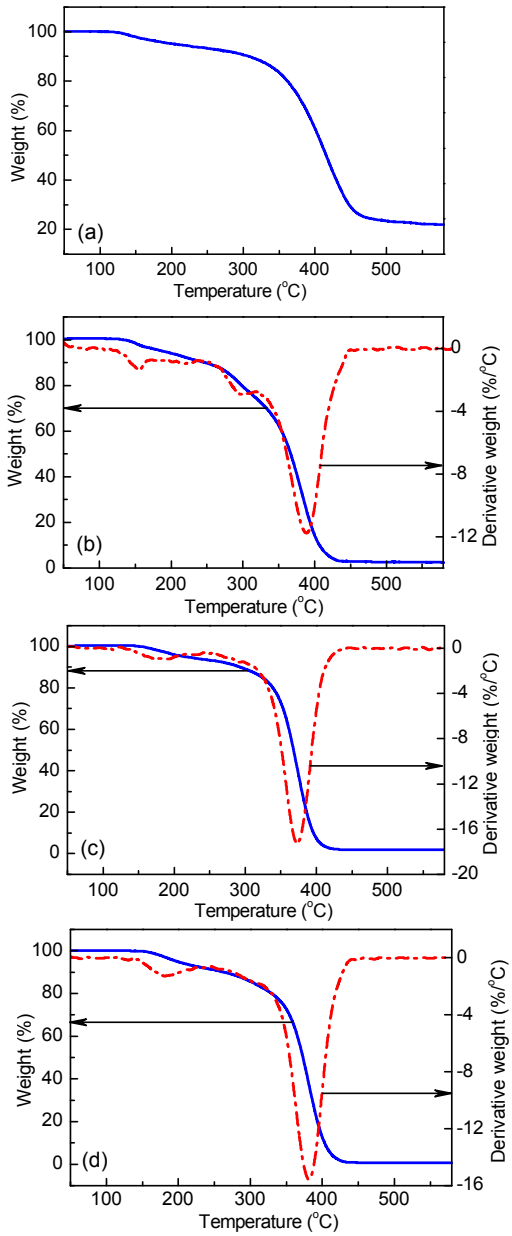

Fig. 6 TGA and DTG curves of sample 6 (a), sample 7 (b), sample 8 (c), and sample 9 (d)

The weight loss from 100 °C to 400 °C is due to decomposition of poly(MMA-*co*-DVB) (Tai *et al.*, 2011). The different weight losses of the particles showed different amounts of the polymer shell. We can see from Fig. 6 that the amount of polymer is about 90%.

3.2.4 Magnetism of the synthesized microspheres

The saturation magnetization curves of the synthesized MPMS were obtained by a SQUID under a magnetic field ranging from −10000 Oe to 10000 Oe at room temperature as shown in Fig. 7.

From Fig. 7 we can see that saturation magnetization of samples 6, 7, 8, and 9 are 9.8 emu/g, 0.75 emu/g, 0.78 emu/g, and 0.9 emu/g, respectively. The lower saturation magnetization of samples 7, 8, and 9 can be ascribed to the lower magnetite content of the magnetic microspheres, which is consistent with the TGA result. This result showed that both the amount and porogen type affect a lot of polymer structure. Besides, the typical characteristics of superparamagnetic behavior which means the magnetism only shows on the condition of an external magnetic field (Mu and Wang, 2015) were observed because from the magnetic curve the coercivity and remanence at room temperature are almost unable to be observed.

3.2.5 Porosity and surface structure of the synthesized microspheres

Pore distribution and structures of the MPMS were determined by Hg intrusion and extrusion methods (Fig. 8).

From the Hg ascending and descending branches, we can get not only pore distribution but also pore structures (Svata, 1972). At the same cumulative intrusion amount (the *Y*-axis value), if the pressure of the intrusion segment is the same as that of the extrusion segment, then the pores are most probably in cylindrical shape or V shape; if the pressure of the intrusion segment is higher than that of the extrusion segment, then the pore shape is similar to that of an ink bottle with smaller neck and bigger cavity (Svata, 1972). From Fig. 8, we can see that the particles synthesized with a good solvent, e.g., toluene, tend to form pores with cylindrical shape or V shape, while a poor solvent helps to form pores with ink bottle shape.

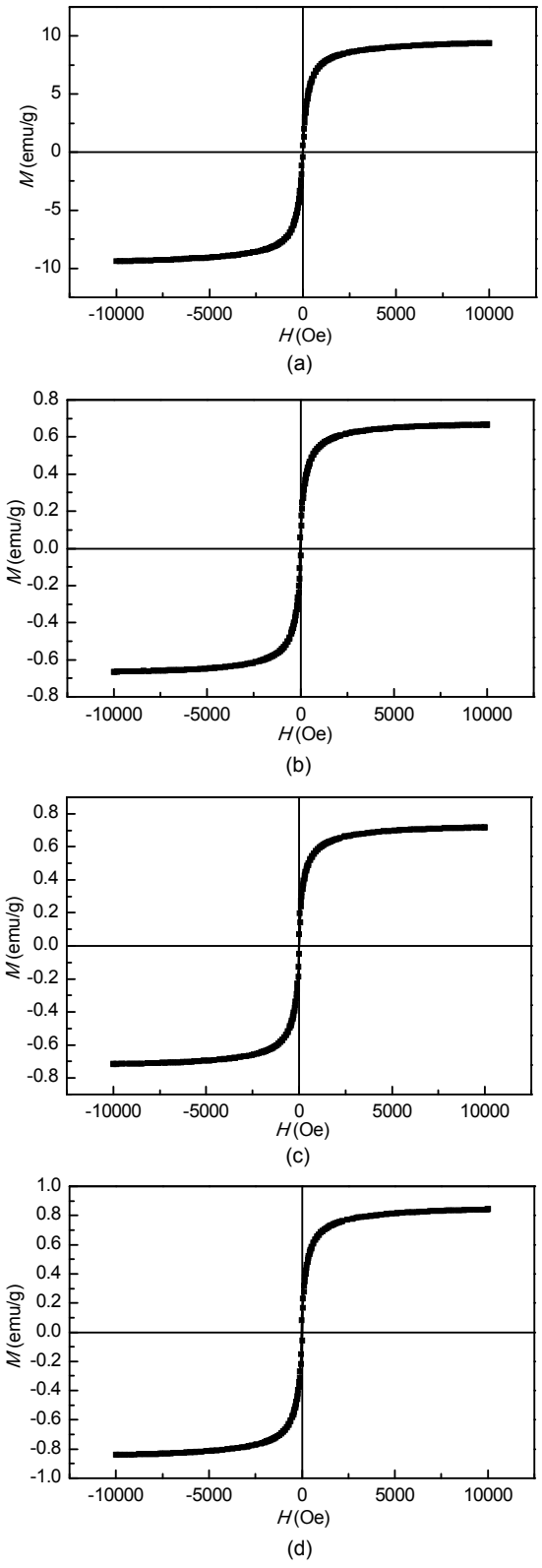

Fig. 7 Magnetic curves obtained by SQUID of sample 6 (a), sample 7 (b), sample 8 (c), and sample 9 (d) at room temperature

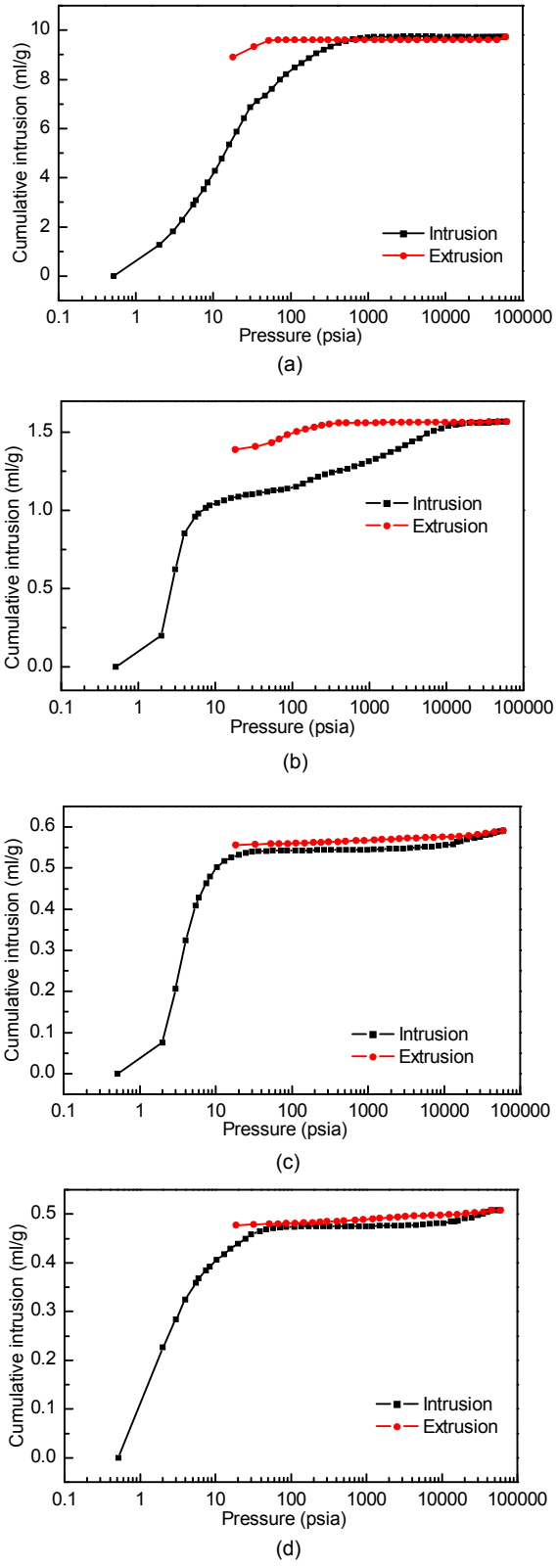

Fig. 8 Hg intrusion-extrusion curves of sample 6 (a), sample 7 (b), sample 8 (c), and sample 9 (d)
Note: 1 psia=6.896 kPa

3.2.6 Adsorption capacity to Rhodamine B of the synthesized microspheres

The standard curve of UV adsorption of Rhodamine B solution is calculated from the adsorption curve of Rhodamine B solution with different concentrations (Fig. 9).

Fig. 10 shows the adsorption of MPMS to Rhodamine B and the desorption effect of ethanol. The insertion is the photograph of the adsorption and desorption phenomena from which we can see clearly the strong adsorption of the synthesized particles to Rhodamine B and the desorption of ethanol from it.

From Fig. 10, we can see that after 4 times using of 5 mg MPMS, the adsorption ability is still very high, which demonstrates the reusability of MPMS.

At last, the quantitative treatment ability of MPMS to Rhodamine B was also examined by the UV absorption method (Fig. 11).

The concentration of the original solution is 2.04×10^{-5} mol/L, and as shown in Fig. 11, with the

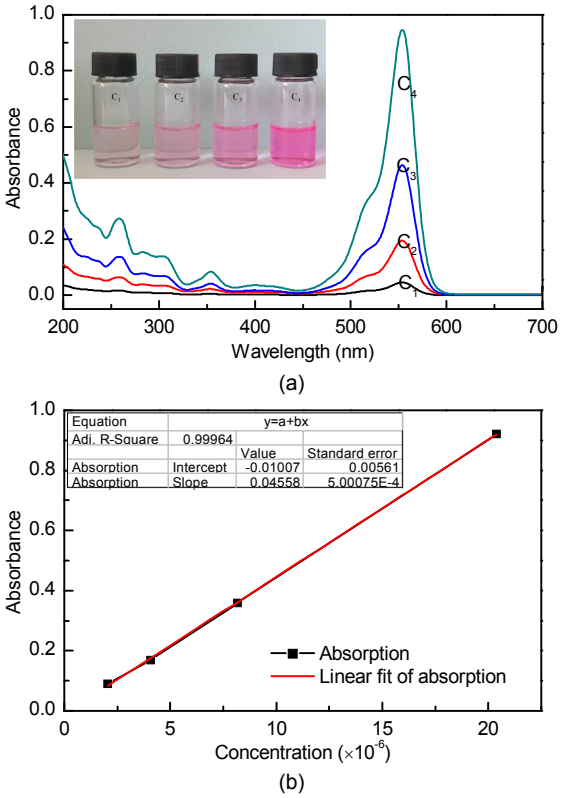

Fig. 9 UV adsorption lines and related photograph of the solution (a) and the standard line of the concentration of Rhodamine B at the adsorption of λ=554 nm (b)

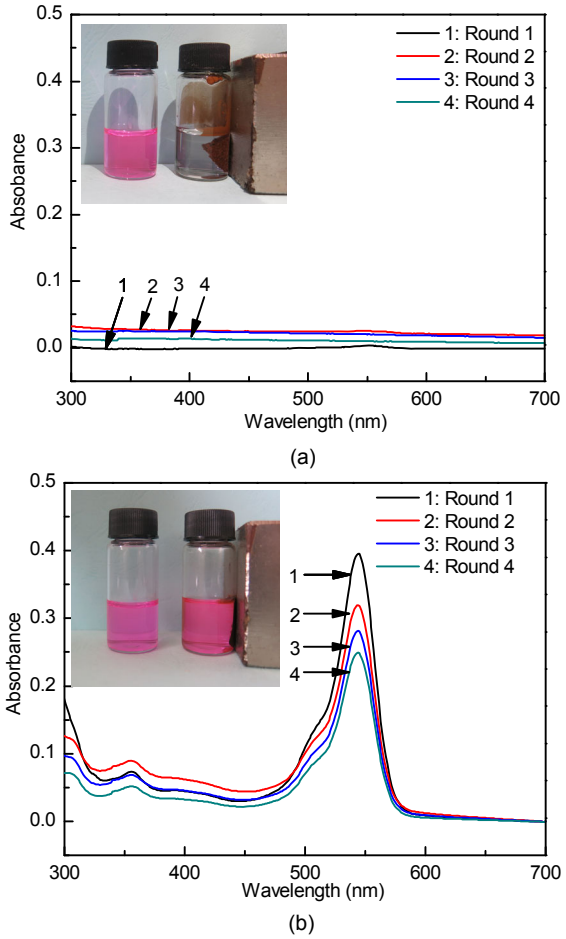

Fig. 10 UV adsorption spectra of the Rhodamine B solution after the treatment with porous spheres (sample 4) (a) and its desorption of ethanol (b)

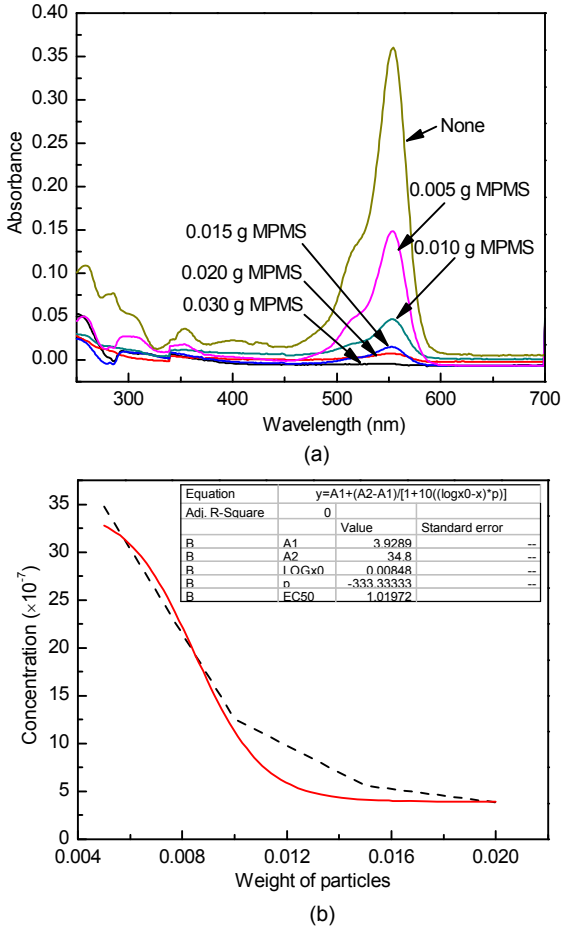

Fig. 11 UV adsorption spectra of the Rhodamine B solution after the treatment with different amounts of MPMS (a) and the adsorption ability of the microspheres to Rhodamine B solution calculated from the UV spectra (b)

increase in the amount of MPMS, the concentration droped and quantitatively, the adsorption ability of MPMS to Rhodamine B is 0.81 mg/g (mg Rhodamine B/g MPMS).

4 Conclusions

Fe_3O_4/poly(MMA-*co*-DVB) MPMS was successfully synthesized. It was found that the crystallinity of Fe_3O_4 was stable during the synthesis of MPMS. The morphology of MPMS, pore distribution, and type were found to be affected by the ratio of MMA to DVB, the porogen type, and the ratio of the porogen to monomer. The microspheres exhibited relatively high adsorption capacity to Rhodamine B due to their pore structure and the polar groups of the surface and also as it has good reusability because of the magnetic core. Thus, a simple approach was developed to synthesize MPMSs with porous and polar surface and magnetic core. These MPMS can have extensive potential applications in many fields, for example, dye and heavy metal contaminant adsorption treatment, immobilization of enzymes, drug-targeted delivery, and biological separation.

References

Adnan, L.A., Yusoff, A.R.M., Hadibarata, T., *et al.*, 2014. Biodegradation of bis-azo dye Reactive Black 5 by white-rot fungus *Trametes gibbosa* sp. WRF 3 and its metabolite characterization. *Water, Air, & Soil Pollution*, **225**(10):1-11. [doi:10.1007/s11270-014-2119-2]

Ahmed, M.A., Khafagy, R.M., Bishay, S.T., *et al.*, 2013. Effective dye removal and water purification using the electric and magnetic $Zn_{0.5}Co_{0.5}Al_{0.5}Fe_{1.46}La_{0.04}O_4$/ polymer core-shell nanocomposites. *Journal of Alloys*

and Compounds, **578**:121-131. [doi:10.1016/j.jallcom.2013.04.182]

Almeida, E.J.R., Corso, C.R., 2014. Comparative study of toxicity of azo dye Procion Red MX-5B following biosorption and biodegradation treatments with the fungi *Aspergillus niger* and *Aspergillus terreus*. *Chemosphere,* **112**:317-322. [doi:10.1016/j.chemosphere.2014.04.060]

Chen, Y.H., Liu, Y.Y., Lin, R.H., *et al.*, 2009. Photocatalytic degradation of *p*-phenylenediamine with TiO_2-coated magnetic PMMA microspheres in an aqueous solution. *Journal of Hazardous Materials*, **163**(2-3):973-981. [doi:10.1016/j.jhazmat.2008.07.097]

Cheng, Z., Zhang, L., Guo, X., *et al.*, 2015. Adsorption behavior of Direct Red 80 and Congo Red onto activated carbon/surfactant: process optimization, kinetics and equilibrium. *Spectrochimica Acta Part A: Molecular and Biomolecular Spectroscopy*, **137**:1126-1143. [doi:10.1016/j.saa.2014.08.138]

Crini, G., 2005. Recent developments in polysaccharide-based materials used as adsorbents in wastewater treatment. *Progress in Polymer Science*, **30**(1):38-70. [doi:10.1016/j.progpolymsci.2004.11.002]

Debnath, S., Ballav, N., Nyoni, H., *et al.*, 2015. Optimization and mechanism elucidation of the catalytic photodegradation of the dyes Eosin Yellow (EY) and Naphthol blue black (NBB) by a polyaniline-coated titanium dioxide nanocomposite. *Applied Catalysis B: Environmental*, **163**:330-342. [doi:10.1016/j.apcatb.2014.08.011]

Filice, S., D'Angelo, D., Libertino, S., *et al.*, 2015. Graphene oxide and titania hybrid Nafion membranes for efficient removal of methyl orange dye from water. *Carbon*, **82**:489-499. [doi:10.1016/j.carbon.2014.10.093]

Fu, J., Chen, Z., Wang, M., *et al.*, 2015. Adsorption of methylene blue by a high-efficiency adsorbent (polydopamine microspheres): kinetics, isotherm, thermodynamics and mechanism analysis. *Chemical Engineering Journal*, **259**:53-61. [doi:10.1016/j.cej.2014.07.101]

Gao, H.J., Zhao, S.Y., Cheng, X.Y., *et al.*, 2013. Removal of anionic azo dyes from aqueous solution using magnetic polymer multi-wall carbon nanotube nanocomposite as adsorbent. *Chemical Engineering Journal*, **223**:84-90. [doi:10.1016/j.cej.2013.03.004]

Garrido-Ramirez, E.G., Theng, B.K.G., Mora, M.L., 2010. Clays and oxide minerals as catalysts and nanocatalysts in Fenton-like reactions-a review. *Applied Clay Science*, **47**(3-4):182-192. [doi:10.1016/j.clay.2009.11.044]

Hameed, B.H., Din, A.T.M., Ahmad, A.L., 2007. Adsorption of methylene blue onto bamboo-based activated carbon: kinetics and equilibrium studies. *Journal of Hazardous Materials*, **141**(3):819-825. [doi:10.1016/j.jhazmat.2006.07.049]

Jarvis, K.L., Majewski, P., 2014. Removal of acid orange 7 dye from water via plasma-polymerized allylamine-coated quartz particles. *Water, Air, and Soil Pollution*, **225**(12):2227. [doi:10.1007/s11270-014-2227-z]

Khoobi, M., Delshad, T.M., Vosooghi, M., *et al.*, 2015. Polyethyleneimine-modified superparamagnetic Fe_3O_4 nanoparticles: an efficient, reusable and water tolerance nanocatalyst. *Journal of Magnetism and Magnetic Materials*, **375**:217-226. [doi:10.1016/j.jmmm.2014.09.044]

Li, D., Jiang, D., Chen, M., *et al.*, 2010. An easy fabrication of monodisperse oleic acid-coated Fe_3O_4 nanoparticles. *Materials Letters*, **64**(22):2462-2464. [doi:10.1016/j.matlet.2010.08.025]

Liang, C.Z., Sun, S.P., Li, F.Y., *et al.*, 2014. Treatment of highly concentrated wastewater containing multiple synthetic dyes by a combined process of coagulation/flocculation and nanofiltration. *Journal of Membrane Science*, **469**:306-315. [doi:10.1016/j.memsci.2014.06.057]

Liu, Q., Wang, L., Xiao, A., *et al.*, 2010. Templated preparation of porous magnetic microspheres and their application in removal of cationic dyes from wastewater. *Journal of Hazardous Materials*, **181**(1-3):586-592. [doi:10.1016/j.jhazmat.2010.05.053]

Luo, S., Duan, L., Sun, B., *et al.*, 2015. Manganese oxide octahedral molecular sieve (OMS-2) as an effective catalyst for degradation of organic dyes in aqueous solutions in the presence of peroxymonosulfate. *Applied Catalysis B: Environmental*, **164**:92-99. [doi:10.1016/j.apcatb.2014.09.008]

Macintyre, F.S., Sherrington, D.C., 2004. Control of porous morphology in suspension polymerized poly-(divinylbenzene) resins using oligomeric porogens. *Macromolecules*, **37**(20):7628-7636. [doi:10.1021/ma0491053]

Mak, S.Y., Chen, D.H., 2004. Fast adsorption of methylene blue on polyacrylic acid-bound iron oxide magnetic nanoparticles. *Dyes and Pigments*, **61**(1):93-98. [doi:10.1016/j.dyepig.2003.10.008]

Mao, J., Jiang, W., Gu, J., *et al.*, 2014. Synthesis of P (St-DVB)/Fe_3O_4 microspheres and application for oil removal in aqueous environment. *Applied Surface Science*, **317**:787-793. [doi:10.1016/j.apsusc.2014.08.191]

Meshko, V., Markovska, L., Mincheva, M., *et al.*, 2001. Adsorption of basic dyes on granular acivated carbon and natural zeolite. *Water Research*, **35**(14):3357-3366. [doi:10.1016/S0043-1354(01)00056-2]

Mu, B., Wang, A., 2015. One-pot fabrication of multifunctional superparamagnetic attapulgite/Fe_3O_4/polyaniline nanocomposites served as an adsorbent and catalyst support. *Journal of Materials Chemistry A*, **3**(1):281-289. [doi:10.1039/C4TA05367B]

Namasivayam, C., Kavitha, D., 2002. Removal of Congo Red from water by adsorption onto activated carbon prepared from coir pith, an agricultural solid waste. *Dyes and Pigments*, **54**(1):47-58. [doi:10.1016/S0143-7208(02)00025-6]

Ning, Y.C., 2000. Structural Identification of Organic Compounds and Organic Spectroscopy. Science Press,

Beijing, China (in Chinese).

Palma-Goyes, R.E., Silva-Agredo, J., Gonzalez, I., *et al.*, 2014. Comparative degradation of indigo carmine by electrochemical oxidation and advanced oxidation processes. *Electrochimica Acta*, **140**:427-433. [doi:10.1016/j.electacta.2014.06.096]

Rabelo, D., Coutinho, F.M.B., 1993. Cosolvency effects of benzyl alcohol and heptane on the formation of macroporous styrene-divinylbenzene copolymers. *Polymer Bulletin*, **31**(5):585-592. [doi:10.1007/BF00297896]

Svata, M., 1972. Determination of pore size and shape distribution from porosymmetric hysteresis curves. *Powder Technology*, **5**(6):345-349. [doi:10.1016/0032-5910(72)80040-8]

Tai, Y.L., Wang, L., Gao, J.M., *et al.*, 2011. Synthesis of Fe_3O_4@poly(methylmethacrylate-*co*-divinylbenzene) magnetic porous microspheres and their application in the separation of phenol from aqueous solutions. *Journal of Colloid and Interface Science*, **360**(2):731-738. [doi:10.1016/j.jcis.2011.04.096]

Tang, M., Zhang, S., Li, X., *et al.*, 2014. Fabrication of magnetically recyclable Fe_3O_4@Cu nanocomposites with high catalytic performance for the reduction of organic dyes and 4-nitrophenol. *Materials Chemistry and Physics*, **148**(3):639-647. [doi:10.1016/j.matchemphys.2014.08.029]

Tang, Q., Lin, J., Wu, Z., *et al.*, 2007. Preparation and photocatalytic degradability of TiO_2/polyacrylamide composite. *European Polymer Journal*, **43**(6):2214-2220. [doi:10.1016/j.eurpolymj.2007.01.054]

Vimonses, V., Lei, S., Jin, B., *et al.*, 2009. Kinetic study and equilibrium isotherm analysis of Congo Red adsorption by clay materials. *Chemical Engineering Journal*, **148**(2-3):354-364. [doi:10.1016/j.cej.2008.09.009]

Wang, M., Cui, S., Yang, X., *et al.*, 2015. Synthesis of g-C_3N_4/Fe_3O_4 nanocomposites and application as a new sorbent for solid phase extraction of polycyclic aromatic hydrocarbons in water samples. *Talanta*, **132**:922-928. [doi:10.1016/j.talanta.2014.08.071]

Wang, S.B., Li, H., Xu, L.Y., 2006. Application of zeolite MCM-22 for basic dye removal from wastewater. *Journal of Colloid and Interface Science*, **295**(1):71-78. [doi:10.1016/j.jcis.2005.08.006]

Yan, T.G., Wang, L.J., 2014. Adsorption of C.I. Reactive Red 228 and Congo Red dye from aqueous solution by amino-functionalized Fe_3O_4 particles: kinetics, equilibrium, and thermodynamics. *Water Science & Technology*, **69**(3):612-621. [doi:10.2166/wst.2013.745]

Zhao, S., Gao, B., Yue, Q., *et al.*, 2014. Effect of Enteromorpha polysaccharides on coagulation performance and kinetics for dye removal. *Colloids and Surfaces A: Physicochemical and Engineering Aspects*, **456**:253-260. [doi:10.1016/j.colsurfa.2014.05.035]

Zolgharnein, J., Bagtash, M., Shariatmanesh, T., 2015. Simultaneous removal of binary mixture of Brilliant Green and Crystal Violet using derivative spectrophotometric determination, multivariate optimization and adsorption characterization of dyes on surfactant modified nano-gamma-alumina. *Spectrochimica Acta Part A: Molecular and Biomolecular Spectroscopy*, **137**:1016-1028. [doi:10.1016/j.saa.2014.08.115]

中文概要

题　目：磁性多孔四氧化三铁/聚（甲基丙烯酸甲酯-*co*-二乙烯基苯）微球的制备、表征及其去除罗丹明 B 的应用研究

目　的：通过悬浮聚合法合成含有 Fe_3O_4 磁性核的多孔聚合物微球，研究不同单体比例、致孔剂类型及用量对所合成磁性微球的形貌影响以发现最佳反应条件，最终将所合成的磁性多孔微球应用于从水溶液中去除阳离子染料罗丹明 B，并证明成功。

方　法：1. 通过改进的悬浮聚合法合成了磁性多孔四氧化三铁/聚（甲基丙烯酸甲酯-*co*-二乙烯基苯）；2. 通过红外及能谱表征产物的组成，使用扫描电镜及透射电镜表征产物的表面及内部形貌，通过热失重分析表征产物的聚合物包覆率，通过 X 射线粉末衍射表征产物的晶型，使用压汞法表征产物的多孔性及孔结构，利用超导量子干涉仪测定产物的磁性能；3. 通过紫外分光光度法验证产物对于罗丹明 B 的吸附及其效果。

结　论：1. 通过改进的悬浮聚合法成功合成磁性多孔四氧化三铁/聚（甲基丙烯酸甲酯-*co*-二乙烯基苯）；2. 表面聚合物的包覆并不影响四氧化三铁的晶型；3. 产物的形貌及孔结构受到单体甲基丙烯酸甲酯与致孔剂二乙烯基苯的比例、致孔剂类型及用量等多方面影响；4. 所合成的产物对于罗丹明 B 有很好的吸附效果，同时具有很好的重复利用性；5. 所合成的聚合物在废水中重金属的去除、酶固定化、药物的靶向释放及生物分离等方面都有潜在应用价值。

关键词：Fe_3O_4/poly(MMA-*co*-DVB)；多孔；染料去除